JOURNAL OF MATERIALS SCIENCE 31 (1996) 2653–2660

Catastrophic fracture induced fracto-emission

HONGLAI TAN, WEI YANG
Department of Engineering Mechanics, Tsinghua University, Beijing 100084, People's Republic of China

Fracto-emissions accompanying crack propagation were observed in recent experiments. The energy impulses during and after each atomistic fracture increment stimulate the fracto-emission. A model of the atomic scale cleavage processes is proposed to formulate a catastrophic fracture theory relevant to these phenomena. A criterion for catastrophic jump of the cleavage potential is applied to representative crystals. We simulate the propagation of the emitted particles along a crack bounded by zigzag surfaces and quantify the long-time delay law of fracto-emissions after fracture.

1. Introduction

Recently experiments on fracture processes have shown the emission of particles, including photons, electrons, ions and neutral species, "during" and "following" the fracture of materials [1, 2]. These phenomena are collectively termed "fracto-emissions" because the material fracture appears to be a prerequisite for their appearance. Fracto-emission can serve as an attractive aid to understand atomic scale fracture processes. The transport of fracto-emissions has proved to be a useful probe of the local environment in materials where that transport is limited by the local geometry. Experiment by Langford *et al.* [3] used the photon emission as a probe of chaotic processes accompanying fracture.

Dickinson *et al.* [1] and Fuhrmann *et al.* [2] gave estim ates that fracto-emissions are caused by the high concentration of energy spikes deposited into a small volume of material during crack propagation. The energy impulse excites particles and creates defects in materials, and consequently results in the emission of excited and reactive species in a gas phase. The mechanism for creating an energy impulse remains equivocal. In the present paper we construct a catastrophic fracture theory to investigate this process. The energy criterion for fracto-emission is formulated. The cleavage model of atom strings embedded in a cracked continuum, as analysed in detail by Tan and Yang [4], is applied to evaluate the energy impulse on bond breaking. For fracture controlled by dislocation emissions (Tan and Yang [5]), similar energy impulses can be revealed as the crack moves forward, although there is no cleavage-like bond breaking during this procedure.

In most cases, the intensities of fracto-emissions reach their peak during the fracture event and decay afterward. However, recent measurements by Dickinson *et al.* [6] show rapid, intense bursts of atomic and molecular emissions that arise *after* the fracture. They attributed these bursts to the energetic emergence ("popout") of dislocations at a free crack surface. We find catastrophic energy release, and consequently emission burst, during the unloading process of cleavage, though this phenomenon has not been addressed in the literature.

Dickinson *et al.* [7] reported measurements of long-time decay from 10^{-2} to 10^{3} s of photon and electron emissions following fracture from several polymeric and inorganic systems. The experiment suggested a strong correlation between the long-time decay and the local structure at the fracture surface. Applying the rough morphology of the crack surfaces, we propose a zigzag crack model to quantify this process. The model simulates a decay law for the fracto-emission intensity consistent with the experiments.

2. Fracto-emissions by catastrophic cleavage processes

2.1. Atom string model for cleavage

We consider an averaging plane strain continuum deformation. The three-dimensional atomic motions (solid particles) can be studied by their projections (shaded images) onto the plane perpendicular to $\mathbf{e}_3$ direction, as depicted in Fig. 1. The current crack tip rests at the atom pair 1 and 1′. The three-dimensional atom string line orients at an angle θ with the $\mathbf{e}_2$ axis. The angle θ reflects the actual three-dimensional lattice structure.

Fig. 2 delineates the plane strain projections of the atom string (which is embedded in the surrounding continuum containing a crack) before and after an atomistic cleavage step. This model simplifies the combined atomistic/continuum configuration proposed by Yang *et al.* [8] and by Tan and Yang [9, 10]. The continuum stress field surrounding the crack tip is symmetric and scaled by the mode I stress intensity factor K_{I}. For the study of an atomistic cleavage process, the continuum in the vicinity of the crack tip can be viewed as linear elastic [9]. In the figure, δ denotes the distance between the neighbouring atom strings along the central crack extension line in the projection plane.

0022–2461

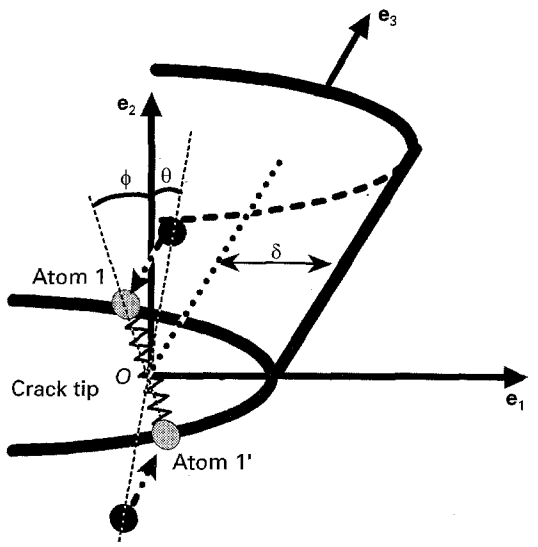

Figure 1 Crack tip model for plane strain problem. Atoms in three-dimensional configuration are projected to the plane perpendicular to the $\mathbf{e}_3$ direction. The solid circles refer to the three-dimensional lattice atoms, the shaded ones refer to the projected atoms.

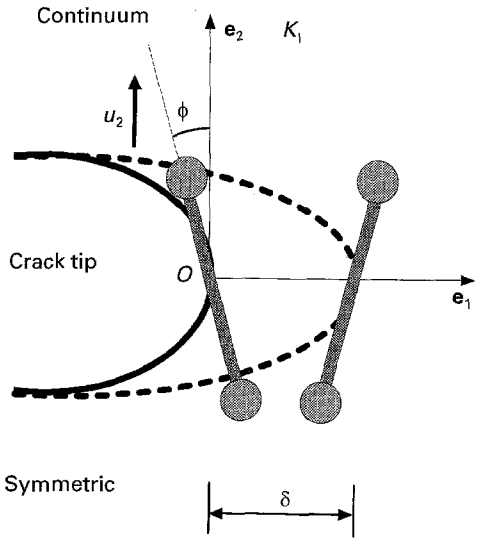

Figure 2 Two-atom string model at a crack tip modelling the cleavage process. The solid line refers to the current crack tip configuration, and the dashed line refers to the subsequent configuration with a crack moving one interatomic distance ahead. The atomic motion interacts with the motion of the surrounding continuum.

The surrounding continuum exerts two effects on the movement of atom 1. One is the stretching effect due to the remote stress intensity factor K_I, which under an equilibrium deformation causes a force F_I^{eq}. Following the derivation of Tan and Yang [4], we have

$$F_I^{eq}(K_I) = 0.818 w \delta^{1/2} K_I \tag{1}$$

where w is the width of the crack front shared by each bonding atom pair. The other effect is the confining effect by the continuum against the atom displacement, described by k_I through the following expression

$$k_I(E') = 0.513 E' w \tag{2}$$

where $E' = E/(1 - \nu^2)$. E is the Young's modulus, and ν is the Poisson's ratio.

As shown in [4] the dynamics governing equation for the motion of atom 1 is

$$m\ddot{u}_2 = -\frac{d}{du_2} U(u_2; K_I, E'), \tag{3}$$

where m is the mass of the atom, and u_2 is the vertical displacement of the atom. The cleavage potential at an equilibrium state has the following expression

$$U(u_2; K_I, E') = \frac{1}{2}\Phi(r(u_2)) - F_I^{eq}(K_I)u_2 + \frac{1}{2}k_I(E')u_2^2 \tag{4}$$

where u_2 is the state variable, and K_I and E' are macroscopic parameters characterizing the loading intensity and the material property. The rapid convergence to an equilibrium state was reasoned by Tan and Yang [4]. The distance between atom 1 and 1' is

$$r(u_2) = [(r_0 \cos\theta + 2u_2)^2 + (r_0 \sin\theta)^2]^{1/2} \tag{5}$$

where r_0 is the stress-free nearest interatomic distance.

The interatomic potential $\Phi(r)$ takes different forms for different kinds of bonding. For ionic crystals, the theory of Born gives

$$\Phi(r) = \frac{A}{r^s} - \alpha_M \frac{e^2}{4\pi\varepsilon_0 r} \tag{6}$$

where s denotes a dimensionless exponent of about 10, A an interatomic bonding constant, α_M the Madelung constant, e the unit of electron charge, and ε_0 the dielectric constant. For crystals with metallic or covalent bonds, we take the simple expression suggested by Cherepanov [11]

$$\Phi(r) = \left[-3\left(\frac{r_0}{r}\right)^6 + 2\left(\frac{r_0}{r}\right)^9 \right] e_0 \tag{7}$$

where e_0 is the reference interaction energy.

During a non-equilibrium bond breaking process, the force acting on atom 1 is denoted as $F_I(t)$, and it varies with time t during the cleavage process. We denote the time interval for the crack tip to move ahead a distance δ as t_{frac} and the force acting on the crack tip atom to cause a catastrophic bond breaking as F_{IC}. Obviously, $F_I(t)$ is bounded above by F_{IC}. Under sustained loading of K_I, $F_I(t)$ increases monotonically with time and converges to F_I^{eq} when t exceeds t_{frac}. The non-equilibrium cleavage potential can be formally written as

$$U(u_2; F_I, E') = \frac{1}{2}\Phi(r(u_2)) - F_I u_2 + \frac{1}{2}k_I(E')u_2^2 \tag{8}$$

This potential is applicable to a nearly quasi-static process prior to fracto-emission.

2.2. Energy impulses induced fracto-emission

The crack tip atomic potential drops when the crack advances. The released potential energy converts into the kinetic energy of the crack tip atoms. Two channels exist to absorb or to diffuse this kinetic

energy. One is through the excitation of fracto-emissions, and the other is through wave propagation. Fracto-emissions will be excited when the energy impulse is sufficiently high and cannot be effectively carried away by wave propagation in the time interval of t_{frac}.

As fracture proceeds, the cracked surface is left in a highly excited state. Vibration excitations with effective surface temperatures in excess of 1000 K may be possible [12]. The high temperature renders fracto-emission easier. As a result, the probability of fracto-emission can be expressed in an Arrhenius form

$$\text{Prob} = \min\left\{\exp\left[\frac{(\Delta E - \hat{E})}{k_B T}\right], 1\right\} \tag{9}$$

where k_B is the Boltzmann's constant, T is the temperature in Kelvin at the crack tip, ΔE is the energy released in a time interval prior to any substantial energy diffusion by wave propagation, and $\hat{E}$ is the energy barrier to bring out a fracto-emission particle. Different particle emissions relate to different physical or chemical reactions, so have different values of $\hat{E}$.

Values of $\hat{E}$ can be estimated from the results of sublimation experiments. Take the example of fracto-emission for NaCl monomers. Experiments [13] indicate that the emission of an NaCl monomer from a defect-free flat surface requires 2.2 eV. The energy required for fracture related emission should be considerably lower than that. The sublimation energy on a cracked surface of NaCl is about 0.25 eV [13].

The available time for fracto-emission, t_{frac}, can be estimated from the crack propagation velocity v_{frac}

$$t_{frac} = \frac{\delta}{v_{frac}} \tag{10}$$

The crack velocity can be estimated from light transmission measurements [14]. In experiments concerning fracto-emissions, this value can vary from very slow (several m s^{-1}) to very fast (hundreds of m s^{-1}). Consequently, the time interval t_{frac} for fracto-emissions ranges from 100 ps (slow cleavage) to 0.2 ~ 1 ps (fast cleavage).

2.3. Catastrophic jump for slow cleavage processes

We now investigate the slow cleavage case where t_{frac} is about 100 ps. This time interval is much larger than the dynamic characteristic time t_{wave} defined by

$$t_{wave} = \frac{a_0}{v_{wave}} \tag{11}$$

where v_{wave} denotes the smallest stress wave speed and a_0 is the crystal lattice parameter. Typical data give the order of t_{wave} in the range of 0.1–0.2 ps. For the slow cleavage case, we have $t_{frac} \gg t_{wave}$, and a quasi-static approximation can be applied to the governing Equation 3. Accordingly, $F_I(t)$ is a slow varying function during the cleavage process, and remains unchanged during bond breaking. Under the applied F_I, the equilibrium atom displacement u_2^{eq} can be solved from

$$-\frac{1}{2} f(r(u_2^{eq})) \frac{dr(u_2^{eq})}{du_2} - F_I + k_1(E') u_2^{eq} = 0 \tag{12}$$

where the interatomic force is given by

$$f(r) = -d\Phi(r)/dr \tag{13}$$

When the solution of Equation 12 satisfies

$$\frac{1}{2} k_f(r(u_2^{eq})) \left(\frac{dr(u_2^{eq})}{du_2}\right)^2 - \frac{1}{2} f(r(u_2^{eq})) \frac{d^2 r(u_2^{eq})}{du_2^2} + K_I(E') > 0 \tag{14}$$

with

$$k_f(r) = -\frac{d}{dr} f(r) \tag{15}$$

the crack tip atom has the minimum potential and stays at a stable configuration. The atomistic configuration is unstable otherwise.

Taking the special case of $a_0 = 4$ Å, $m = 1.0 \times 10^{-25}$ kg, $e_0 = 2.22$ eV and a simple cubic lattice structure, one gets $E' = 84.2$ GPa provided the expression of $\Phi(r)$ is given by Equation 7. The $u_2^{eq}(F_I)$ curve for this representative case is shown in Fig. 3. This curve shows the fold catastrophe with the fold points at A and B, and they give two critical values F_{IC1} and F_{IC2}. When $F_I < F_{IC2}$ or $F_I > F_{IC1}$, Equation 12 possesses a unique solution. When $F_{IC2} < F_I < F_{IC1}$, three solutions coexist. The reference force in the figure is $F_0 = 0.818\, a_0^2 E'$. The solid curves in Fig. 3 refer to stable states and the dashed curves to unstable states. Their distinction is made by Condition 14.

Fig. 3 reveals a negative hysteresis loop during the loading and unloading cycles. When the load F_I increases from a low value up to F_{IC1}, the crack tip atoms will catastrophically jump outward from state A to state A', as shown in Fig. 3. On the other hand, when

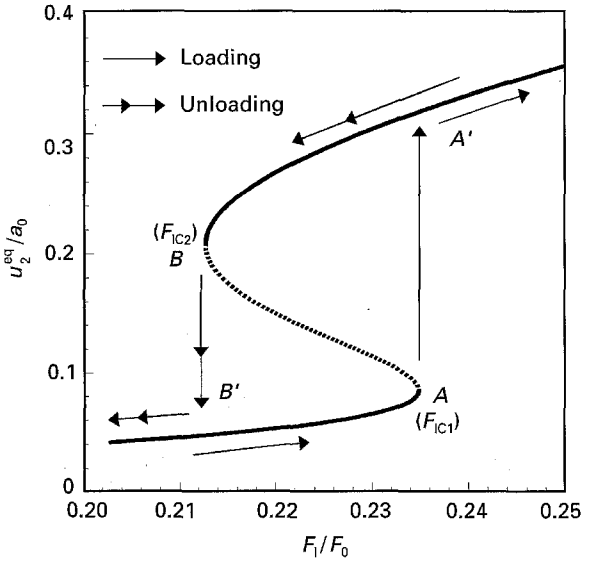

Figure 3 Catastrophic jump of the equilibrium position of the crack tip atom during the cleavage process. The solid curves refer to stable states and the dashed curves to unstable states.

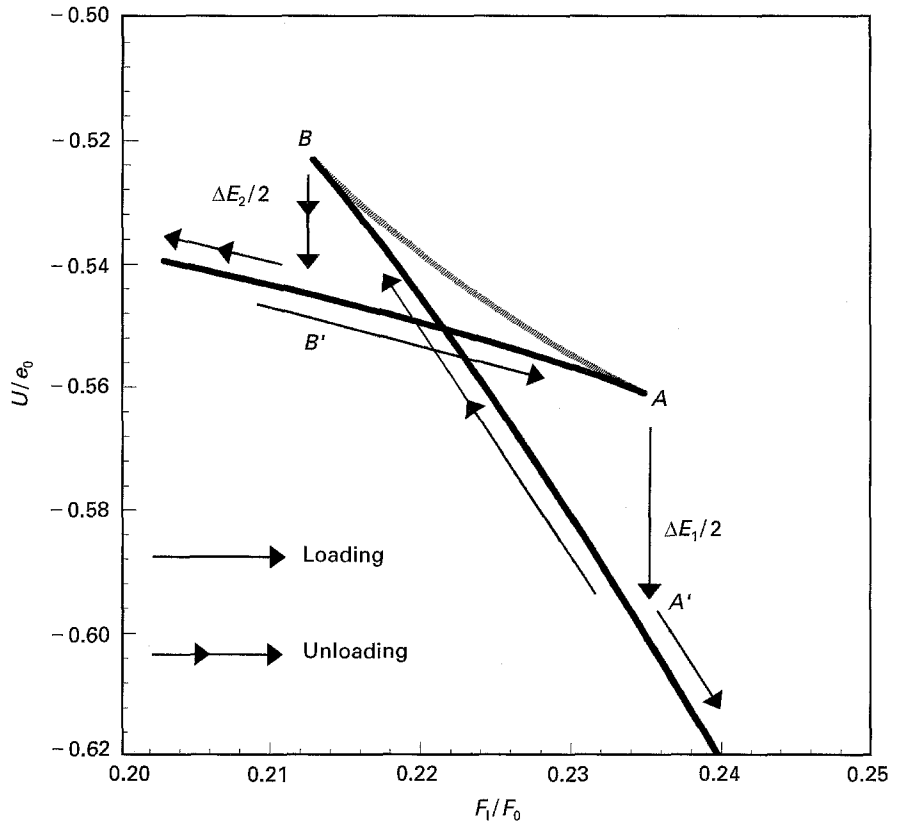

Figure 4 Catastrophic release of the cleavage potential energy. The solid curves refer to stable states and the dashed curves to unstable states.

the applied force reduces from a high value down to F_{IC2}, the crack tip atoms will catastrophically jump inward from state B to state B'. The unilateral jumping amplitude for one atom ranges from $0.15 \sim 0.25a_0$. These two catastrophic changes of atom behaviour give sudden potential energy releases during and after fracture, as observed in the experiment of Dickinson *et al.* [6].

We show in Fig. 4 the catastrophic release of cleavage potential for the same representative case. Consistent with the displacement process, the catastrophic jump of the system from state A to state A' gives an energy release of $\Delta E_1 = 0.18$ eV. In unloading the catastrophic jump from state B to state B' gives an energy release of $\Delta E_2 = 0.10$ eV.

The time duration for this catastrophic energy release can be estimated from

$$t_{\text{jump}} = \Delta u_2 / v_{\text{jump}} \tag{16}$$

where Δu_2 is the jump value of the vertical displacement at catastrophe. In deriving Equation 16, we assume atom 1 separates from atom 1' by uniform acceleration to achieve v_{jump}, the jumping velocity of the bond-broken atom. The potential energy jump ΔE_1 of the atom pair is transformed into the kinetic energy mv_{jump}^2 of two symmetric atoms at the crack tip. Therefore, v_{jump} can be evaluated as

$$v_{\text{jump}} = \left(\frac{\Delta E_1}{m}\right)^{1/2} \tag{17}$$

Combining Equations 16 and 17, one finds the time interval in the opening jump for the crack tip atom pair is about 0.18 ps, provided the unilateral vertical jump is $\Delta u_2 = 0.25a_0$. This jump time is relatively short, so that the energy impulse released during the catastrophe cannot be effectively taken away by wave dispersion and can be supplied to cause fracto-emissions.

Fracto-emissions hardly occur without the presence of a catastrophic jump. In the time duration of $(0, t_{\text{frac}})$ before a catastrophic jump, Fig. 4 shows a continuous potential release. However, this energy release is too slow to cause fracto-emissions. The energy release rate can be estimated as approximately $(U_0 - U_A)/t_{\text{frac}}$, where U_0 is the potential at the reference configuration and U_A is the potential before the catastrophic point A. The energy release rate during the catastrophe, namely $\Delta E_1/t_{\text{jump}}$, is about 360 times higher than the average energy release rate before the catastrophic jump. Therefore, the energy impulse to stimulate the fracto-emission can only be generated by the catastrophic jumps.

Under a prescribed F_I value, the solution u_2^{eq} for Equation 12 depends critically on E'. Fig. 5 shows the surface $u_2^{eq}(E', F_I)$. This graph has the structure of a cusp catastrophe. From terms in catastrophe theory, the curve on the surface where the upper and lower sheets fold over into the middle sheet is called the fold-curve. The projection of this curve onto the horizontal controlling plane forms the bifurcation set. Although the fold curve is a smooth curve, the bifurcation set has a sharp point C, forming a cusp, as shown in Fig. 6. Two continuous lines L_1 and L_2 comprising the bifurcation set outline the main thresholds for sudden behavioural change of the system.

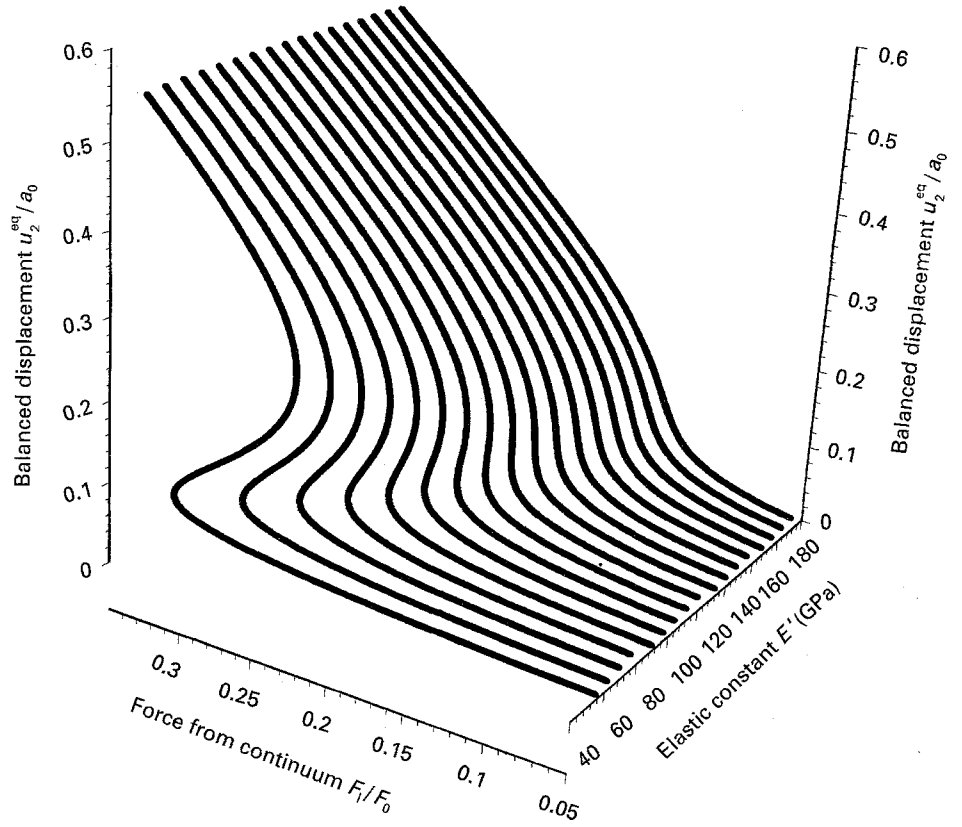

Figure 5 Three-dimensional portrait of the surface $u_2^{eq}(E', F_I)$ shows a cusp catastrophe. Each line in the surface corresponds to a specific material characterized by the elastic constant E'.

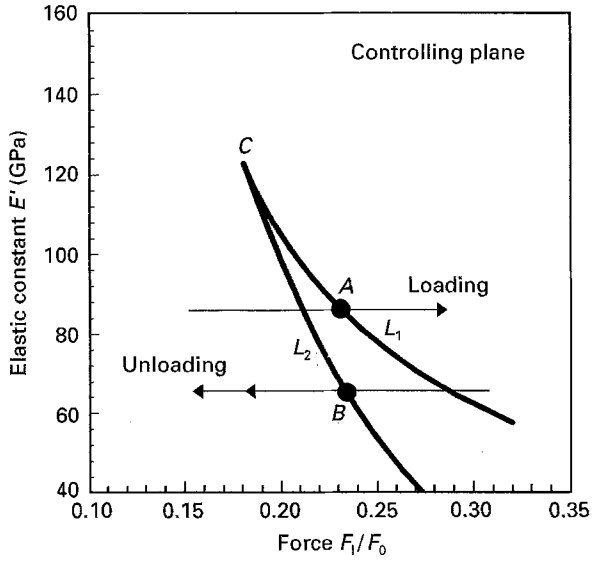

Figure 6 Bifurcation set curve of $u_2^{eq}(E', F_I)$. The bifurcation set has a sharp cusp point C.

We now deduce the equation for the bifurcation set. Along the three-dimensional fold curve, one has

$$\frac{\partial u_2^{eq}}{\partial E'} = \infty \quad \text{and} \quad \frac{\partial u_2^{eq}}{\partial F_I} = \infty \tag{18}$$

These two equations share the same requirement that

$$\frac{1}{2} k_f(r(u_2^{eq})) \left(\frac{dr(u_2^{eq})}{du_2}\right)^2 - \frac{1}{2} f(r(u_2^{eq})) \frac{d^2 r(u_2^{eq})}{du_2^2} + k_I(E') = 0 \tag{19}$$

Combining Equations 12 and 19 we define the curves L_1 and L_2. During the loading induced cleavage process, a catastrophic jump would occur if the loading path (at a prescribed E') travels across the branch L_1 from left to right. During the unloading process, a reverse catastrophic jump would occur if the unloading path travels across branch L_2 from right to left.

The cusp point C provides a critical value for the material parameter E'

$$E'_C = \max_{0 < u_2^{eq} < \infty} \left\{ \frac{0.975}{w} \left[-k_f(r(u_2^{eq})) \left(\frac{dr(u_2^{eq})}{du_2}\right)^2 + f(r(u_2^{eq})) \frac{d^2 r(u_2^{eq})}{du_2^2} \right] \right\} \tag{20}$$

The criterion for the material to have a catastrophic jump is

$$E' < E'_C \tag{21}$$

Table I lists relevant data for several representative materials based on the present theory for slow cracking. Values of a_0, A, s, E' for case (a) are taken from experimental data reported in [15, 16]. Values of a_0, e_0, E' for cases (b)–(d) are calculated from experimental data in [17, 18]. Some materials listed in the table are ductile under normal conditions and the fracture process is mainly controlled by dislocation emissions. In the cases involving laminates assembled by alternating sub-micron ductile and brittle layers, see Hsia *et al.* [19], the dislocation confinement suppresses the ductile fracture mode and cleavage occurs when the tensile stress at the crack tip reaches the theoretical strength. In the case of high loading rate,

TABLE I Fracto-emission analysis on representative materials

(a) Ionic crystals of NaCl structure, cleavage system (001) [100]
$\theta = 0$, $\delta = a_0$, $w = a_0$, $r_0 = a_0$

Crystal	a_0 (nm)	A (eV(nm)^s)	s	E' (GPa)	E'_C (GPa)	ΔE_1 (eV)	ΔE_2 (eV)
LiF	0.201	1.03×10^{-4}	6.20	108	314	3.18	1.05
NaCl	0.282	2.91×10^{-5}	8.38	43.4	109	2.30	0.926

(b) Metallic crystal of fcc structure, cleavage system (001) [110]
$\cos\theta = \frac{2^{1/2}}{2}$, $\delta = \frac{2^{1/2}}{4} a_0$, $w = \frac{2^{1/2}}{4} a_0$, $r_0 = \frac{2^{1/2}}{2} a_0$

Crystal	a_0 (nm)	e_0 (eV)	E' (GPa)	E'_C (GPa)	Fracto-emissions
Cu	0.255	0.391	147	102	No
Al	0.286	0.359	79.8	66.6	No

(c) Metallic crystal of bcc structure, cleavage system (001) [100]
$\cos\theta = 3^{-1/2}$, $\delta = \frac{1}{2} a_0$, $w = \frac{1}{2} a_0$, $r_0 = \frac{3^{1/2}}{2} a_0$

Crystal	a_0 (nm)	e_0 (eV)	E' (GPa)	E'_C (GPa)	Fracto-emissions
Fe	0.248	0.780	231	155	No
W	0.274	1.57	446	230	No

(d) Covalent crystal of diamond cubic structure, cleavage system (111) [0$\bar{1}$1]
$\cos\theta = 1$, $\delta = \frac{2^{1/2}}{4} a_0$, $w = \frac{6^{1/2}}{4} a_0$, $r_0 = \frac{3^{1/2}}{4} a_0$

Crystal	a_0 (nm)	e_0 (eV)	E' (GPa)	E'_C (GPa)	ΔE_1 (eV)	ΔE_2 (eV)
C	0.154	3.59	1.09×10^3	2.46×10^3	0.644	0.660
Si	0.235	2.16	154	416	0.764	0.488
Ge	0.245	1.96	123	334	0.688	0.445

some apparently ductile materials will cleave, as demonstrated by Tan and Yang [9]. The results in Table I indicate that we can hardly observe fracto-emission in metallic crystals. The fracto-emission for ionic and covalent crystals can be easily observed. The catastrophic energy release under these materials varies from 0.4–3.2 eV, sufficient to induce fracto-emission.

2.4. Fast cleavage processes

In the fast cleavage case, v_{frac} is comparable to the wave propagation velocity so that $t_{wave} \approx t_{frac}$. The potential energy releases continuously and rapidly in the short time period t_{frac}. This contrasts with the slow cleavage case where the energy release rate is negligible most of the time and has an impulse in the incident of catastrophe. For the fast cleavage case, the total energy released, when the crack tip advances one inter-atomic distance, is comparable to that released during a catastrophic jump for the slow cleavage case. This continuous energy release will drive successive fracto-emissions.

Similar impulses of energy release can be predicted for dislocation emission processes, under the dislocation emission band model by Tan and Yang [5].

3. Long-time decay of fracto-emissions

3.1. Zigzag crack model for fracto-emission

Scanning tunnelling microscope observations of LiF fracture surfaces indicate that they can be very rough on the nanoscopic scale [6]. A simple quantitative description for an irregular surface was to model it as a zigzag surface, as shown in the schematic profiles in [20]. Using the zigzag profile model, we present here a numerical simulation of the fracto-emission process channelled by the cracked surfaces. The result suggests that the long-lasting tail seen in the photon emissions is caused by the zigzag character of crack surfaces.

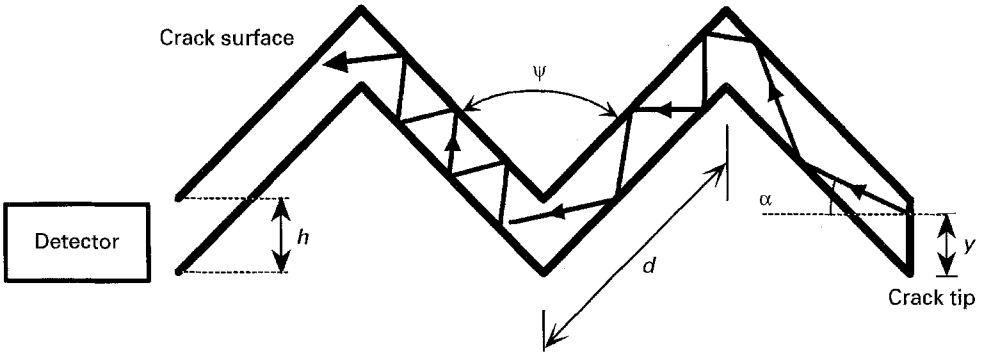

Figure 7 Zigzag crack profile model. Fracto-emission particles bounce at the irregular surface.

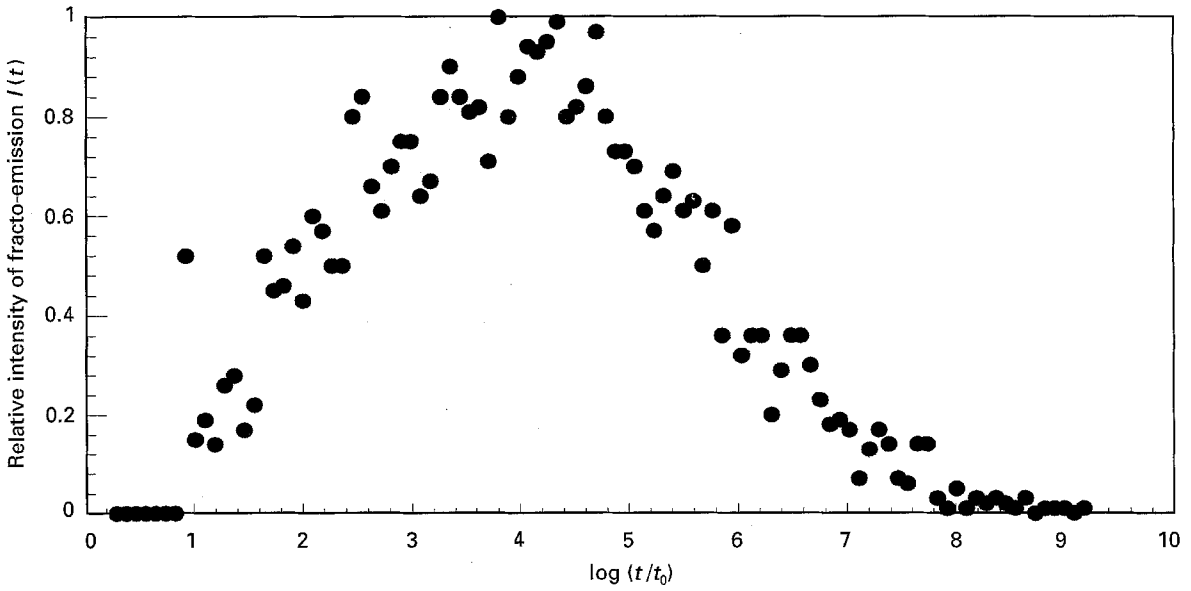

Figure 8 Numerical simulation result for the long-time decay of the fracto-emission intensity in zigzag crack surfaces.

We propose the regular zigzag profile as in Fig. 7. In the figure, Ψ and d represent the angle and the step length of the zigzag, and h denotes the crack separation. The fracto-emission generated at the crack tip will travel along the narrow zigzag crack. The emitted particles hit on the crack and reflect, causing the time delay before they are recorded by the detector. We assume no energy lost in the reflection process and the interaction of the emitted particles with the crack surface costs little time. We take the fracto-emission generation site, described by the parameter y, and the emitting angle, α, to be random. The particles fly in the crack with a constant velocity. Under the above simplifications, we calculated the time duration for the particle escaping from the crack tip to reach the detector.

3.2. Long-time decay estimate

Fig. 8 shows the result calculated by the zigzag crack model. In the simulation we take crack parameters to be $d = 2\,\mu\text{m}$, $h = 20\,\text{nm}$, $\Psi = 60°$, and the length of the crack to be $L = 2\,\text{mm}$. The emitting angle α takes random values within $(-90°, 90°)$, and the emitting position y takes random values within $(0, h)$.

If the crack is ideally flat, after averaging different emission angles α, the time for the particles to fly out of the crack is

$$t_0 = \frac{\pi L}{2v_{\text{emit}}} \tag{22}$$

where v_{emit} is the velocity of the emitted particle. We simulate the propagation process of 5000 particles along the crack under a random emission. The particle beam intensity $I_0(t)$ is defined as

$$I_0(t) = \lim_{\Delta t \to 0} \frac{N(t, \Delta t)}{\Delta t} \tag{23}$$

where $N(t, \Delta t)$ is the number of the particles collected by the detector during an infinitesimal time interval $[t - \Delta t/2, t + \Delta t/2]$. Taking the maximum value of the intensity to be $I_{0\text{m}}$, we define the relative emission intensity as

$$I(t) = I_0(t)/I_{0\text{m}} \tag{24}$$

From the figure we observe that the fracto-emission reaches its peak on the time scale of $63.7t_0$ following the fracture, translating to about 0.4 ms, if v_{emit} is taken as $500\,\text{m}\,\text{s}^{-1}$. It decays for a relatively long time. In 4 s after the fracture we can still observe the fracto-emissions.

Fig. 9 shows a log–log plot of the after-peak fracto-emission intensity versus time. The relation between

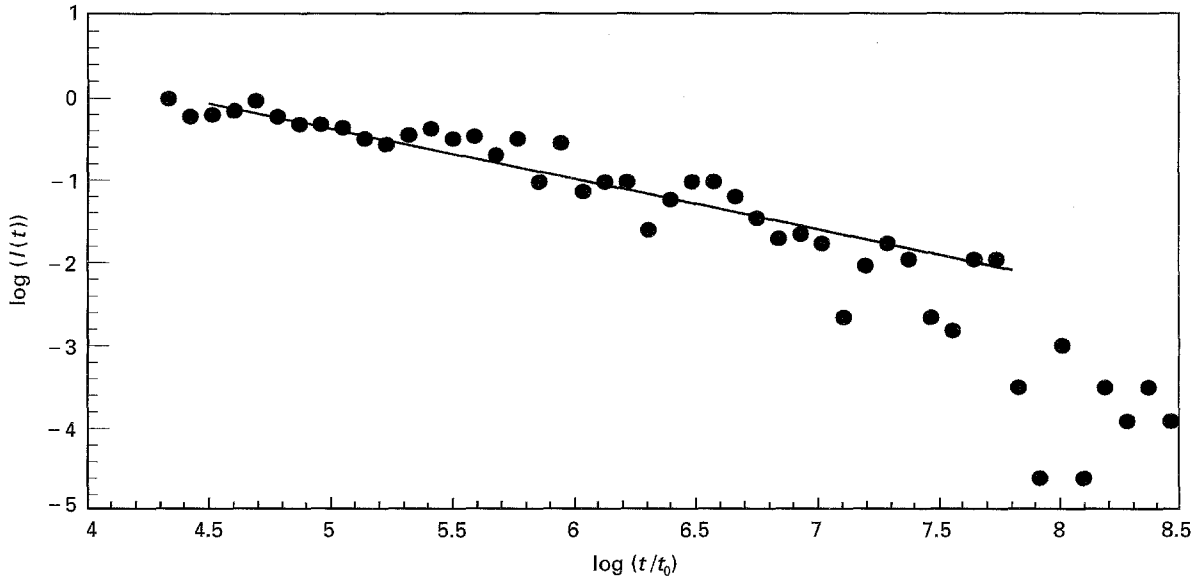

Figure 9 Log–log curve of the fracture emission intensity versus time for the after-peak decay period.

$\log(I(t))$ and $\log(t/t_0)$ is roughly linear. From the figure we get

$$\log I(t) = \lambda - \beta \log(t/t_0) \tag{25}$$

From the slope of the log–log curve we can estimate that $\beta = 0.63$. This gives an emission decay law of

$$I(t) \propto \frac{1}{t^{\beta}} \tag{26}$$

The value of β depends on Ψ and h/d, which are controlled by the material properties and the load amplitude. We expect that β increases as either Ψ or h/d increases. Using a random walk description of the recombination process, Dickinson *et al.* [7] got a relation similar to Equation 26 from the experimental data. In the experiments, they obtained β as 0.83 for photon emission following the fracture of neat epoxy, and 0.79 for electron emission of Kevlar-filled epoxy.

4. Concluding remarks

Fracto-emissions accompanying crack propagation are studied in an atomistic model of fracture. The following conclusions are reached:

1. Energy impulses may be released during the cleavage processes when the crack tip atom pair undergoes loading or unloading. These energy releases account for the fracto-emissions during and after fracture. In the slow cleavage case, the debonding of metallic crystals cannot induce a catastrophic energy jump, and thus cannot cause fracto-emissions. The cleavages of ionic and covalent crystals show obvious energy impulses. Criterion for the fracto-emission is formulated. Energy impulses are also released during dislocation emission processes.

2. Long-time decay of the fracto-emission may attribute to the zigzag morphology of the crack surfaces. Fracto-emission through a regular zigzag is simulated to estimate the interception intensity at the detector. An inverse power law for the emission intensity versus decaying time correlates to the simulation data. This decay law is similar to that obtained from experiments.

Acknowledgement

This research project is jointly supported by the National Natural Science Foundation of China, and by the State Education Commission of China.

References

1. J. T. DICKINSON, E. E. DONALDSON and M. K. PARK, *J. Mater. Sci.* **16** (1981) 2897.
2. J. FUHRMANN, L. NICK, J. T. DICKINSON and L. C. JENSEN, *J: Appl. Polym. Sci.* **48** (1993) 2123.
3. S. C. LANGFORD, Z. MA and J. T. DICKINSON, *J. Mater. Res.* **4** (1989) 1272.
4. H. TAN and W. YANG (1995) *Int. J. Fract.* accepted.
5. *Idem*, **78** (1995) *J. Appl. Phys.* submitted.
6. J. T. DICKINSON, L. C. JENSEN, S. C. LANGFORD and J. P. HIRTH, *J. Mater. Res.* **6** (1991) 112.
7. J. T. DICKINSON, S. C. LANGFORD and L. C. JENSEN, *ibid.* **8** (1993) 2921.
8. W. YANG, H. TAN and T. F. GUO, *Model. Simul. Mater. Sci. Eng.* **2** (1994) 767.
9. H. TAN and W. YANG, *Acta Mech. Sinica* **10** (1994) 150.
10. *Idem, ibid.* **10** (1994) 237.
11. G. P. CHEREPANOV, "Mechanics of Brittle Fracture" (Nauka Press, Moscow, 1974).
12. P. J. MILLER, C. S. COFFEY and V. F. DEVOST, *J. Appl. Phys.* **59** (1986) 913.
13. D. W. SHORT, R. A. RAPP and J. P. HIRTH, *J. Chem. Phys.* **57** (1972) 1381.
14. K. A. ZIMMERMAN, S. C. LANGFORD, J. T. DICKINSON and R. P. DION, *J. Polym. Sci.* **31** (1993) 1229.
15. M. P. TOSI, in "Solid State Physics", Vol. 16, edited by F. Seitz and D. Turnbull (Academic, New York, 1964) p. 1.
16. J. J. GILMAN, "Fracture" (John Wiley, New York, 1959).
17. "Smithells Metals Reference Book", edited by E. A. Bandes (Butterworths, London, 1983).
18. C. S. BARRETT and T. B. MASSALSKI, "Structure of Metals" (McGraw-Hill, New York, 1966).
19. K. J. HSIA, Z. SUO and W. YANG, *J. Mech. Phys. Solids* **42** (1994) 877.
20. M. COSTER and J. L. CHERMANT, *Inter. Metals Rev.* **28** (1983) 228.

Received 15 February
and accepted 19 November 1995